PAPER

Check for updates

Tuning the charge carrier mobility in few-layer PtSe2 films by Se : Pt ratio

Jana Hrdá, [ab] Valéria Tašková,[a] Tatiana Vojteková,[ac] Lenka Pribusová Slušná,[a] Edmund Dobročka,[a] Igor Píš, [d] Federica Bondino, [d] Martin Hulman[a] and Michaela Sojková [*a]

Recently, few-layer $PtSe_2$ films have attracted significant attention due to their properties and promising applications in high-speed electronics, spintronics and optoelectronics. Until now, the transport properties of this material have not reached the theoretically predicted values, especially with regard to carrier mobility. In addition, it is not yet known which growth parameters (if any) can experimentally affect the carrier mobility value. This work presents the fabrication of horizontally aligned $PtSe_2$ films using one-zone selenization of pre-deposited platinum layers. We have identified the Se : Pt ratio as a parameter controlling the charge carrier mobility in the thin films. The mobility increases more than twice as the ratio changes in a narrow interval around a value of 2. A simultaneous reduction of the carrier concentration suggests that ionized impurity scattering is responsible for the observed mobility behaviour. This significant finding may help to better understand the transport properties of few-layer $PtSe_2$ films.

Any material used in high-speed electronics needs to fulfil basic requirements, including a high current on/off switch ratio and high charge carrier mobility for fast operation.[1] Layered 2D transition metal dichalcogenide (TMDC) materials with tuneable band gap and transitional behaviour have considerable potential in this area.[2] TMDCs contain over 40 combinations of transition metal and chalcogenides.[3] Platinum diselenide ($PtSe_2$) belongs to a group of noble-TMDCs, which naturally occurs in the 1T phase.[4] $PtSe_2$ has been predicted as an exceptional material, and in addition, experiments proved its outstanding properties, such as widely tuneable band gap, air stability and high carrier mobility. Single-layer to few-layer $PtSe_2$ is a p-type semiconductor, thicker or bulk $PtSe_2$ shows a semi-metallic character.[5,6] It has been confirmed, that $PtSe_2$ also has optoelectronic performance[7] and photocatalytic activities.[5,6] This extends its possible applications in photodetection[8] or quick-response gas sensing.[9,10] Avsar *et al.*[11] showed that atomic-scale defects could transform non-magnetic 2D crystals into magnetic phases. Using first-principles calculations they suggest that a platinum vacancy defect yields antiferro- (ferro-) magnetic ordering in mono- (bi-) layer $PtSe_2$. For all the

applications mentioned above, high quality and large-area $PtSe_2$ films are necessary.

Several possible fabrication methods of monolayer and few-layer $PtSe_2$ have been developed. Yan *et al.* used molecular beam epitaxy to create high-quality epitaxial thin $PtSe_2$ films with a controllable thickness.[12] This method is outstanding for creating large-size single-crystalline films on various substrates. On the other hand, this method is less suitable for large-scale device fabrication. Chemical vapour deposition[13,14] and direct selenization of thin platinum films (also called thermally assisted conversion-TAC)[6,15] are extensively used to fabricate $PtSe_2$ films on the nanometres thickness range. This method is suitable for preparing large-area films. However, nanocrystals are oriented randomly, yet no long-range ordering within the layer has been experimentally achieved. This is one of the limiting factors for much lower charge carrier mobility than it was predicted.

As we have already mentioned above, $PtSe_2$ is a promising material for application in electronics. The charge carrier mobility of $PtSe_2$ has been predicted to be one of the highest among TMDCs.[16] However, the experimentally measured carrier mobility of $PtSe_2$ is much lower than the theoretically predicted value.[2] The mobility strongly depends on the scattering phenomena within the material. Intrinsic mobility is determined by scattering caused by lattice vibrations.[1] For 2D materials in general, several factors including charge impurity, structural defects or surface optical phonons scattering, dominate the charge transport.[17,18] For example, point defects typically lower the carrier mobility or degrade mechanical

a Institute of Electrical Engineering, SAS, Dúbravská cesta 9, 841 04 Bratislava, Slovakia. E-mail: michaela.sojkova@savba.sk

b Faculty of Electrical Engineering and Information Technology, Slovak University of Technology, Ilkovičova 3, 812 09 Bratislava, Slovakia

c Faculty of Mathematics, Physics and Informatics, Comenius University in Bratislava, Mlynská dolina F2, 842 48, Bratislava, Slovak Republic

d IOM-CNR, Laboratorio TASC, S.S. 14 km 163.5, 34149 Basovizza, Trieste, Italy

properties of 2D materials.[19] Fabrication method also strongly influences the film quality as well as charge carrier mobility values. The highest values were obtained on $PtSe_2$ flakes peeled off from bulk crystals using a scotch tape-based mechanical exfoliation. Zhao *et al.*[16] fabricated a few-layer device on SiO_2/Si substrate exhibiting a semiconducting behaviour with high room-temperature electron mobility ($210 \ cm^2 \ V^{-1} \ s^{-1}$) in a back-gated configuration. Xu *et al.*[20] demonstrated the controllable doping in $PtSe_2$ few-layer films prepared by selenization. Depending on the growth conditions, they fabricated both n-type and p-type $PtSe_2$ films of various thicknesses.[20] The films showed FET mobility of 14 and $15 \ cm^2 \ V^{-1} \ s^{-1}$ for p-type and n-type FETs, respectively. Selenization of pre-deposited platinum layers leads to $PtSe_2$ films exhibiting p-type semiconducting behaviour with hole mobility values up to $13 \ cm^2 \ V^{-1} \ s^{-1}$.[21] However, after the fabrication of FET structure, the field effect mobility decrease to $0.3 \ cm^2 \ V^{-1} \ s^{-1}$.

This paper presents the fabrication of few-layer $PtSe_2$ films by one-zone selenization of a pre-deposited platinum layer. We studied how nitrogen flow during the selenization process affects the chemical composition, structural, and electrical transport properties of the final $PtSe_2$ films. In contrast, the temperature, heating rate, selenization time, and initial thickness of Pt pre-deposited layers were constant. To analyse the structural and chemical properties of prepared $PtSe_2$ films we used the combination of X-ray photoelectron spectroscopy (XPS), X-ray diffraction (XRD) and Raman spectroscopy. The charge carrier mobility of the samples was determined from the Hall-effect measurement. We found a correlation between the selenium concentration in the sample and its carrier mobility. The charge carrier mobility values scale linearly with Se : Pt ratio close to 2.

Experimental

PtSe₂ fabrication

$PtSe_2$ thin films were prepared by a two-step method on the top of the *c*-plane (0001) sapphire substrate. The substrate dimensions were $10 \times 10 \ mm^2$. At first, Pt films were prepared using DC magnetron sputtering in Ar atmosphere (10^{-3} mbar) from a platinum target at room temperature. The DC power and emission current were set to 580 W and 0.18 A, respectively. The thickness of the as-prepared Pt films was set by the rotation speed of a sample holder. Further, the pre-deposited Pt layers were selenized in a custom-designed CVD chamber.[22] The substrate and Se powder are placed in the same position in the center of the furnace. The temperature of the substrate and powder is the same during the growth.[23,24] This is in contrast to the standard CVD method, where the reaction takes place in a two-zone furnace with selenium powder and Pt substrate heated at different temperatures. Annealing temperature (550 °C), annealing time (30 min) and heating rate ($25 \ °C \ min^{-1}$) stay unchanged while the nitrogen flow rate ranged from 20 to 350 sccm.

Characterization

Raman. Raman measurements were performed in a confocal Raman microscope (Alpha 300R, WiTec, Germany). An excitation laser with a 532 nm wavelength and a laser power as low as 1 mW was used to avoid any beam damage. The scattered Raman signal was collected by a $50\times$ (NA = 0.8) microscope objective and detected by a Peltier-cooled EMCCD camera. For dispersing the Raman spectra, a blazed grating with 1800 grooves per mm was employed. The spectral resolution of the entire Raman system is about $0.75 \ cm^{-1}$. The Raman spectra were acquired at ambient conditions.

XPS. Synchrotron radiation photoelectron spectroscopy was performed using the BACH beamline at the Elettra synchrotron in Trieste, Italy. The beamline was equipped with a Scienta R3000 hemispherical analyser at an angle of 60° respective to the X-ray incidence direction. The spectra were recorded in a normal emission geometry, with light linearly polarized in the horizontal plane. The core-level spectra were measured at a photon energy of 1200 eV with a total instrumental resolution of 0.5 eV. Binding energies were calibrated to Au $4f_{7/2}$ peak (84.0 eV) measured on a clean gold reference. Pt 4f and Se 3d core levels were decomposed into their spectral components using Voigt line shapes and a Shirley-type background. To calculate the atomic concentrations, the areas of photoemission peaks were corrected for the photoionization cross-sections,[25,26] inelastic mean free paths determined by TPP-2M formula, and analyser transmission function.[27] The samples were degassed in vacuum at a temperature of 250 °C for 10 minutes before the measurements.

Structural analyses. The structural analysis of $PtSe_2$ layers was performed with a diffractometer Bruker D8 DISCOVER. The diffractometer was equipped with a rotating anode (CuKα) working at the power of 12 kW. X-ray diffraction (XRD) in a symmetrical $\theta/2\theta$ configuration was used to study the crystal structure of the thin films. X-ray reflectivity (XRR) was used to determine the thickness of $PtSe_2$ layers. The crystallographic orientation and the film texture were studied by an azimuthal (φ-scan) measurement.

Electrical characterization. The Hall coefficient and the resistivity were measured by the van der Pauw (vdP) method. The charge carrier mobility was then calculated from these quantities. The measurement configuration consists of: (i) an electromagnet to set the magnetic field up to 1T by a high power source, (ii) a current source Keithley 2400 to set and hold the current on a constant value, and (iii) a multimeter Keithley 2700 to measure the resistance and Hall voltage. Indium contacts were used.

Results and discussion

A series of $PtSe_2$ few-layer films were prepared using selenization of 1 nm thick platinum layer on a *c*-plane sapphire substrate. Annealing temperature, time, and heating rate were similar for all experiments while the nitrogen flow rate varied from 20 up to 350 sccm. The crystal structure of as-prepared $PtSe_2$ films was determined by XRD measurements in a symmetrical $\theta/2\theta$ configuration (Fig. 1(a)). Only a 001 diffraction of the hexagonal 1T $PtSe_2$ phase was visible in the pattern, meaning the layers are aligned horizontally with the c-axis perpendicular to the substrate. The presence of the Laue
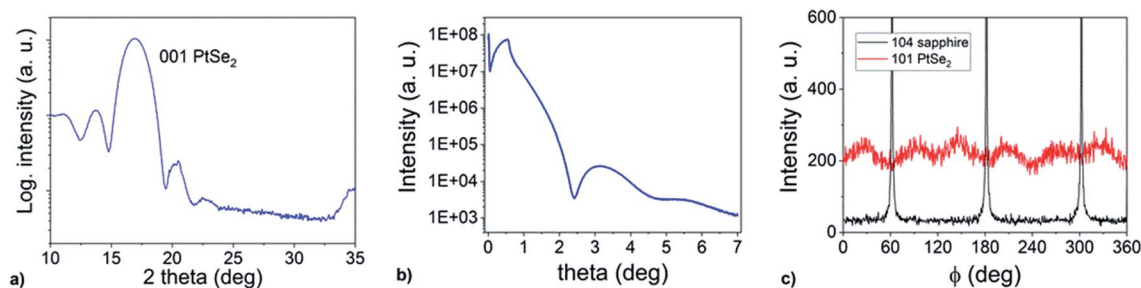
Fig. 1 (a) Typical XRD pattern of PtSe$_2$ film prepared by selenization of 1 nm thick Pt layer at 550 °C during 30 min. (b) Typical XRR spectra of PtSe$_2$ film prepared by selenization of 1 nm thick Pt layer at 550 °C during 30 min. (c) Corresponding φ-scan of 101 diffraction of PtSe$_2$ and 104 diffraction of sapphire.
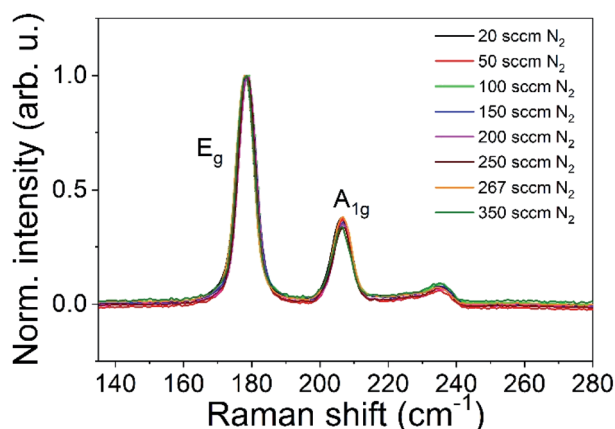

Fig. 2 Normalized Raman spectra of PtSe$_2$ films prepared by selenization of 1 nm thick Pt layer at 550 °C during 30 min with different nitrogen flow rates.

revealed the in-plane crystallographic orientation of the films (Fig. 1(c)). The presence of recognizable maxima indicates that the layers tend to grow epitaxially. However, the maxima are broad suggesting that the in-plane disorder is still present in the sample. Compared with our previous work,[22] peaks have relatively low intensity due to the small sample thickness. The orientation of the layers on the substrate reflects the relative position of the diffraction maxima in the φ-scans of sapphire (black curve in Fig. 1(b)) and PtSe$_2$. From these positions, we can conclude that the hexagonal lattice of PtSe$_2$ is rotated by 30° with respect to the substrate lattice.

Fig. 2 shows Raman spectra of PtSe$_2$ films prepared at 550 °C/30 min using different nitrogen flow rates. The vibration modes belonging to PtSe$_2$ are visible in spectra, concretely E$_g$ mode, which occurs at around 175 cm^{-1} and the A$_{1g}$ mode at approximately 207 cm^{-1}. The spectra are normalized to the E$_g$ line intensity. The A$_{1g}$/E$_g$ intensity ratio increases as the number of PtSe$_2$ layers increases.[29] Since no systematic changes were observed in the A$_{1g}$/E$_g$ ratio, the nitrogen flow rate does not have any noticeable impact on the thickness of the resulting PtSe$_2$ films. The broad and less intense band at around 230 cm^{-1} is assigned to an overlap between two longitudinal optical modes.[29] The shape of the band reflects the thickness of the PtSe$_2$ layer and does not change with the nitrogen flow, confirming the conclusion drawn from the A$_{1g}$/E$_g$ intensity ratio.

The electrical measurements were performed on as-prepared films without patterning. The indium contacts were cold pressed into the corners of a sample. The Hall coefficient and

oscillations on both sides of the dominant 001 diffraction proves the high crystallinity and homogenous thickness of the films. There was no significant difference between patterns using various N$_2$ flow rates. The thickness of as-prepared films was calculated from Laue oscillations and from X-ray reflectivity measurements (Fig. 1(b)) using DIFFRAC.LEPTOS software.[22] All the films have a similar thickness (4 ± 0.5 nm) corresponding to 8 ± 1 monolayers of PtSe$_2$.[28] Azimuthal (φ-scan) measurements of 101 diffraction of PtSe$_2$ and 104 diffraction of sapphire

Table 1 Electrical properties of PtSe$_2$ films prepared by selenization of 1 nm thick Pt layer at 550 °C during 30 min with different nitrogen flow rates

Nitrogen flow rate (sccm)	Hall mobility μ (cm^2 V^{-1} s^{-1})	Concentration of charge carriers (cm^{-2})	Hall constant (cm^2/As)	Se : Pt ratio (1200 eV)
20	20.3	1.1884×10^{14}	5.2522×10^{4}	2
50	14	1.7468×10^{14}	3.5731×10^{4}	1.971
100	15.4	1.4144×10^{14}	4.4130×10^{4}	1.979
150	23.19	8.30×10^{13}	7.50×10^{4}	2.002
200	18.1	1.4761×10^{14}	4.2283×10^{4}	1.988
250	27.1	1.0739×10^{14}	5.8122×10^{4}	2.035
267	24.4	6.72×10^{13}	9.29×10^{4}	2.015
350	10.8	3.5220×10^{14}	1.7722×10^{4}	1.971

Fig. 3 Typical XPS spectra of PtSe$_2$ films prepared by selenization of 1 nm thick Pt layer at 550 °C during 30 min.
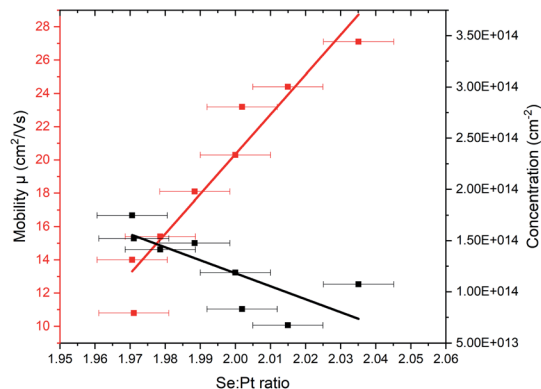

Fig. 4 Se : Pt ratio *vs.* charge carrier mobility and carrier concentration of PtSe$_2$ films prepared by selenization of 1 nm thick Pt layer at 550 °C during 30 min with different N$_2$ flow rate. The solid lines are a linear fits to the experimental values. Error bars represent uncertainty in XPS peak background removal.

the resistivity of the PtSe$_2$ samples were measured by the van der Pauw (vdP) method. At first, conductivity (σ) measurements were performed in vdP configuration. From the measurements in the magnetic field, we estimated the Hall coefficient R_H and charge carrier concentration. The charge carrier mobility μ_H was afterwards calculated from these quantities as $\mu_H = (R_H \times \sigma)$. The polarity of Hall the coefficient determines the type of conductivity. For all as-prepared PtSe$_2$ films showed p-type conductivity. The calculated charge carrier mobility values range from 10.8 to 27.1 cm^2 V^{-1} s^{-1} (Table 1) for the films prepared with different N$_2$ flow rates.

Results from the Hall measurements listed in Table 1 show no clear correlation between the nitrogen flow rate and carrier mobility. Next, we performed synchrotron-radiation XPS measurements with a photon energy of 1200 eV to estimate the films' chemical composition. Fig. 3 shows typical Pt 4f and Se 3d spectra of the films prepared at 550 °C/30 min. The binding energies of the main peaks, 73.07 ± 0.05 eV for Pt 4f$_{7/2}$ and 54.40 ± 0.03 eV for Se 3d$_{5/2}$, are in good agreement with the reported values for PtSe$_2$.[29,30] We found the Se : Pt ratio to be 2.1 ± 0.2. To reduce the uncertainty originating from the cross-sections,[27,31] the Se : Pt atomic ratios were re-scaled to the value obtained for the sample prepared at the lowest nitrogen flow rate. The calculated values are shown in Table 1.

We can see from the table that the charge carrier mobility values are different for different Se : Pt ratio. Xu *et al.*[20] studied the influence of the growth parameters on the electronic properties of PtSe$_2$ films. They showed that the slow cool-down process with a continuous supply of Se precursor enables a complete (over) selenization. Se vacancies can be filled at high temperature in such a process, which resulted in p-type mobility with Se : Pt ratio of about 2.45. On the other hand, the selenization process ends quickly for rapid cooling as the temperature rapidly drops down. For this process, they obtained n-type PtSe$_2$ with Se : Pt ratio of about 1.96. However, the field effect mobility values were almost the same for both types of the films (14 and 15 cm^2 V^{-1} s^{-1} for p-type and n-type FETs, respectively). In contrast, the use of the different N$_2$ flow rates did not significantly change the Se : Pt as in the above-mentioned method. For our films, Se : Pt ranged from 1.97 to 2.03. In all the samples presented here, holes are dominating charge carriers.

When we analysed the values of the charge carrier mobility, Se : Pt ratio and the N$_2$ flow rate, no convincing dependence can be deduced from Table 1. However, we found a correlation between Se : Pt ratio and the charge carrier mobility and charge carrier concentration. Fig. 4 demonstrates the dependence of carrier mobility and concentration on the Se : Pt ratio. The mobility had increased more than twice when Se : Pt increased in a relatively narrow range from 1.97 to 2.03. In contrast, the charge carrier concentration decreases as the Se : Pt is growing. Thus, mobility increases when the carrier concentration gets reduced. Such mobility *vs.* concentration relationship is due to the scattering of mobile charge carriers on ionized impurities. The smaller the concentration, the larger the scattering time and, consequently, carrier mobility.[32]

Conclusions

In conclusion, we report on the chemical, structural and electrical transport properties of few-layer PtSe$_2$ films grown on a *c*-plane sapphire substrate using selenization of pre-deposited platinum layers. The nitrogen flow rate was the only parameter changed during PtSe$_2$ growth. Other parameters such as Pt thickness, heating rate, annealing temperature, and process time, stayed unchanged. The structural characteristics and the

thickness of the films show no sensitivity to the nitrogen flow rate. Similarly, the charge carrier mobility also reveals no convincing dependence on the flow rate, although it ranges from 10.8 up to 27.1 $cm^2 V^{-1} s^{-1}$. On the other hand, we found a clear correlation between carrier mobility and Se : Pt ratio in the films. The charge carrier mobility increases with increasing Se : Pt ratio. At the same time, the carrier concentration decreases, meaning the ionized impurity scattering is likely responsible for the observed mobility *vs.* Se : Pt dependence. We may conclude that even though the nitrogen flow rate does not appear to control the structural and transport properties of as-grown films directly, we have identified the Se : Pt ratio as a parameter that controls the charge carrier mobility.

Author contributions

MS, JH and VT performed the experimental syntheses and characterizations of $PtSe_2$ layers; ED performed the XRD measurements and interpretation of the results; TV and LPS performed the Raman characterization; IP and FB performed the XPS measurements and interpretation of the results; MS, JH and VT performed electrical measurements; JH and MS supervised the project and wrote the manuscript. All authors discussed the results and commented on the manuscript.

Conflicts of interest

There are no conflicts to declare.

Acknowledgements

Notes and references

1 S. H. Mir, V. K. Yadav and J. K. Singh, *ACS Omega*, 2020, **5**, 14203–14211.

2 Y. Gong, Z. Lin, Y.-X. Chen, Q. Khan, C. Wang, B. Zhang, G. Nie, N. Xie and D. Li, *Nano-Micro Lett.*, 2020, **12**, 174.

3 M. Chhowalla, H. S. Shin, G. Eda, L.-J. Li, K. P. Loh and H. Zhang, *Nat. Chem.*, 2013, **5**, 263–275.

4 E. Chen, W. Xu, J. Chen and J. H. Warner, *Mater. Today Adv.*, 2020, **7**, 100076.

5 A. Kandemir, B. Akbali, Z. Kahraman, S. V. Badalov, M. Ozcan, F. Iyikanat and H. Sahin, *Semicond. Sci. Technol.*, 2018, **33**, 085002.

6 Y. Wang, L. Li, W. Yao, S. Song, J. T. Sun, J. Pan, X. Ren, C. Li, E. Okunishi, Y.-Q. Wang, E. Wang, Y. Shao, Y. Y. Zhang, H. Yang, E. F. Schwier, H. Iwasawa, K. Shimada, M. Taniguchi, Z. Cheng, S. Zhou, S. Du, S. J. Pennycook, S. T. Pantelides and H.-J. Gao, *Nano Lett.*, 2015, **15**, 4013–4018.

7 C. Yim, N. McEvoy, S. Riazimehr, D. S. Schneider, F. Gity, S. Monaghan, P. K. Hurley, M. C. Lemme and G. S. Duesberg, *Nano Lett.*, 2018, **18**, 1794–1800.

8 Q. Wang, J. Lai and D. Sun, *Opt. Mater. Express*, 2016, **6**, 2313–2327.

9 M. Sajjad, E. Montes, N. Singh and U. Schwingenschlögl, *Adv. Mater. Interfaces*, 2017, **4**, 1600911.

10 E. Norouzzadeh, S. Mohammadi and M. Moradinasab, *Sens. Actuators, A*, 2020, **313**, 112209.

11 A. Avsar, C.-Y. Cheon, M. Pizzochero, M. Tripathi, A. Ciarrocchi, O. V. Yazyev and A. Kis, *Nat. Commun.*, 2020, **11**, 4806.

12 M. Yan, E. Wang, X. Zhou, G. Zhang, H. Zhang, K. Zhang, W. Yao, N. Lu, S. Yang, S. Wu, T. Yoshikawa, K. Miyamoto, T. Okuda, Y. Wu, P. Yu, W. Duan and S. Zhou, *2D Mater.*, 2017, **4**, 045015.

13 Z. Wang, Q. Li, F. Besenbacher and M. Dong, *Adv. Mater.*, 2016, **28**, 10224–10229.

14 J. Xie, D. Zhang, X.-Q. Yan, M. Ren, X. Zhao, F. Liu, R. Sun, X. Li, Z. Li, S. Chen, Z.-B. Liu and J.-G. Tian, *2D Mater.*, 2019, **6**, 035011.

15 C. Yim, K. Lee, N. McEvoy, M. O'Brien, S. Riazimehr, N. C. Berner, C. P. Cullen, J. Kotakoski, J. C. Meyer, M. C. Lemme and G. S. Duesberg, *ACS Nano*, 2016, **10**, 9550–9558.

16 Y. Zhao, J. Qiao, Z. Yu, P. Yu, K. Xu, S. P. Lau, W. Zhou, Z. Liu, X. Wang, W. Ji and Y. Chai, *Adv. Mater.*, 2017, **29**, 1604230.

17 S. Kim, A. Konar, W.-S. Hwang, J. H. Lee, J. Lee, J. Yang, C. Jung, H. Kim, J.-B. Yoo, J.-Y. Choi, Y. W. Jin, S. Y. Lee, D. Jena, W. Choi and K. Kim, *Nat. Commun.*, 2012, **3**, 1011.

18 Z. Yu, Z.-Y. Ong, Y. Pan, Y. Cui, R. Xin, Y. Shi, B. Wang, Y. Wu, T. Chen, Y.-W. Zhang, G. Zhang and X. Wang, *Adv. Mater.*, 2016, **28**, 547–552.

19 H. Zheng, Y. Choi, F. Baniasadi, D. Hu, L. Jiao, K. Park and C. Tao, *2D Mater.*, 2019, **6**, 041005.

20 H. Xu, H. Zhang, Y. Liu, S. Zhang, Y. Sun, Z. Guo, Y. Sheng, X. Wang, C. Luo, X. Wu, J. Wang, W. Hu, Z. Xu, Q. Sun, P. Zhou, J. Shi, Z. Sun, D. W. Zhang and W. Bao, *Adv. Funct. Mater.*, 2019, **29**, 1805614.

21 L. Ansari, S. Monaghan, N. McEvoy, C. Ó. Coileáin, C. P. Cullen, J. Lin, R. Siris, T. Stimpel-Lindner, K. F. Burke, G. Mirabelli, R. Duffy, E. Caruso, R. E. Nagle, G. S. Duesberg, P. K. Hurley and F. Gity, *npj 2D Mater. Appl*, 2019, **3**, 33.

22 M. Sojková, E. Dobročka, P. Hutár, V. Tašková, L. Pribusová Slušná, R. Stoklas, I. Píš, F. Bondino, F. Munnik and M. Hulman, *Appl. Surf. Sci.*, 2021, **538**, 147936.

23 M. Sojková, P. Siffalovic, O. Babchenko, G. Vanko, E. Dobročka, J. Hagara, N. Mrkyvkova, E. Majková, T. Ižák, A. Kromka and M. Hulman, *Sci. Rep.*, 2019, **9**, 2001.

24 M. Sojková, K. Vegso, N. Mrkyvkova, J. Hagara, P. Hutár, A. Rosová, M. Čaplovičová, U. Ludacka, V. Skákalová, E. Majková, P. Siffalovic and M. Hulman, *RSC Adv.*, 2019, **9**, 29645–29651.

25 D. E. Parry, *Rapid Commun. Mass Spectrom.*, 1994, **8**, 579.

26 J. J. Yeh and I. Lindau, *At. Data Nucl. Data Tables*, 1985, **32**, 1–155.

27 G. Drera, G. Salvinelli, J. Åhlund, P. G. Karlsson, B. Wannberg, E. Magnano, S. Nappini and L. Sangaletti, *J. Electron Spectrosc. Relat. Phenom.*, 2014, **195**, 109–116.

28 W. Jiang, X. Wang, Y. Chen, G. Wu, K. Ba, N. Xuan, Y. Sun, P. Gong, J. Bao, H. Shen, T. Lin, X. Meng, J. Wang and Z. Sun, *InfoMat*, 2019, **1**, 260–267.

29 M. O'Brien, N. McEvoy, C. Motta, J.-Y. Zheng, N. C. Berner, J. Kotakoski, K. Elibol, T. J. Pennycook, J. C. Meyer, C. Yim, M. Abid, T. Hallam, J. F. Donegan, S. Sanvito and G. S. Duesberg, *2D Mater.*, 2016, **3**, 021004.

30 Y. Wang, L. Li, W. Yao, S. Song, J. T. Sun, J. Pan, X. Ren, C. Li, E. Okunishi, Y.-Q. Wang, E. Wang, Y. Shao, Y. Y. Zhang, H. Yang, E. F. Schwier, H. Iwasawa, K. Shimada, M. Taniguchi, Z. Cheng, S. Zhou, S. Du, S. J. Pennycook, S. T. Pantelides and H.-J. Gao, *Nano Lett.*, 2015, **15**, 4013–4018.

31 M. P. Seah, I. S. Gilmore and S. J. Spencer, *J. Electron Spectrosc. Relat. Phenom.*, 2001, **120**, 93–111.

32 D. Chattopadhyay and H. J. Queisser, *Rev. Mod. Phys.*, 1981, **53**, 745–768.